Numerical implementation of the coupled criterion: matched asymptotic and full finite element approaches

Aurélien Doitrand, Eric Martin, Dominique Leguillon

Numerical implementation of the coupled criterion: matched asymptotic and full finite element approaches

Aurélien Doitrand[1*], Eric Martin[2], Dominique Leguillon[3]

[1] *Université Grenoble-Alpes - CNRS UMR 5266, SIMaP, F-38000 Grenoble, France*

[2] *Laboratoire des Composites Thermo-Structuraux, CNRS UMR 5801, Université de Bordeaux, F-33600, Pessac, France*
martin@lcts.u-bordeaux.fr

[3] *Institut Jean le Rond d'Alembert, Sorbonne Université, Centre National de la Recherche Scientifique, UMR 7190, F-75005 Paris, France*
dominique.leguillon@upmc.fr

Abstract

An implementation of the coupled criterion (CC) for crack initiation simulation in the commercial finite element (FE) code Abaqus/Standard is proposed. This finite fracture mechanics approach allows crack initiation to be modeled by fulfilling simultaneously a stress and an energy conditions, which results in the determination of the loading level and crack length at initiation. Two procedures are considered and compared: the first one relies on matched asymptotic expansions while the second one is based on full FE calculations. The asymptotic approach is computationally more efficient than the second one since it requires less calculations to be performed. However, it is restricted to cases for which the crack initiation length remains small compared to the smallest characteristic dimensions of the studied structure. For such cases, both methods leads to similar results as illustrated by crack initiation modeling of notched specimen under three point bending. The provided source codes and the tutorials help understanding and applying the CC for crack initiation modeling.

Keywords: Coupled criterion; Crack initiation; Brittle fracture; Finite element method.

1. Introduction

Among various methods available for brittle fracture modeling such as, *e.g.*, cohesive zone models [1, 2, 3, 4], models based on damage mechanics [5, 6] or phase-field models for fracture [7, 8, 9], the coupled criterion (CC) [10, 11] in the framework of Finite Fracture Mechanics (FFM) [12, 13, 14] proved its ability and efficiency to predict crack initiation in a broad range of materials and configurations. A detailed review of the CC applications was presented by Weissgraeber *et al.* [15]. The principle of the CC is the simultaneous fulfillment of a stress and an energy condition for crack initiation prediction. Coupling both conditions allows determining the initiation loading and crack length. A main advantage of the CC is that it basically requires only two fracture parameters, namely the material strength and fracture toughness which are physical quantities that can be determined experimentally.

*corresponding author, aurelien.doitrand@grenoble-inp.fr

The CC can be implemented through two different methods. The first one, initially proposed by Leguillon [10], relies on the matched asymptotic (MA) expansion procedure proposed by Leguillon and Sanchez-Palencia [16]. The MA approach consists in focusing only on a domain around the initiation crack location so as to compute the energy and the stress conditions without considering the whole specimen or structure. The boundary conditions imposed to the domain around the crack location are asymptotic displacement or stress fields corresponding to the stress concentrator under investigation (*e.g.* sharp or blunted crack, V-notch, hole). Therefore, it relies on the assumption that the initiation crack location is far enough from the structure boundary or other features that may influence these displacement/stress fields. In the second approach, referred to as the full finite element (FFE) approach, the whole structure under consideration is modeled. Compared to the FFE approach, the MA one is usually more computationally efficient since it requires less calculations. For instance, in the case of a sharp V-notch loaded in mode I, only one finite element (FE) calculation is needed [10, 17, 18] whereas several calculations are necessary for the FFE approach. However, the asymptotic approach is only valid if the crack length remains small compared to the characteristic structure dimensions [19]. Moreover, the MA approach allows computing the initiation configuration but is unable to deal with unstable crack propagation that possibly occurs after initiation, which can be accounted for using the FFE approach [15, 20, 21, 22, 23, 24]. Some authors compared the MA and FFE implementation of the CC. For instance Yosibash *et al.* [18] showed that the potential energy variations computed by both approaches for a sharp V-notch were close to each other (difference less than 1%) for small enough cracks, and that this difference was larger for larger cracks. Priel *et al.* [25] obtained similar results in the case of a blunted V-notch. Martin *et al.* [19] showed that the range of validity of the asymptotic approach may be determined by ensuring that the material characteristic length $L_{\text{mat}} = \frac{EG_{\text{c}}}{\sigma_{\text{c}}^2}$ (where E is the material Young's modulus, G_{c} the fracture energy and σ_{c} the tensile strength) is small enough compared to the characteristic dimension of the structure ($L_{\text{mat}} < 0.05h$ for the studied case of a bimaterial specimen submitted to a four point bending test, where h is the substrate thickness).

The theory of the CC can be found in several papers in the case of MA (*e.g.*, [17, 18, 25, 26, 27]) and FFE approaches (*e.g.*, [19, 20, 28, 29, 30, 31]). However, contrary to the other approaches for brittle fracture modeling cited previously (such as cohesive zone or phase field models), dedicated tools are not available for the CC application in commercial FE codes. The objective of this paper is to fill this gap and to provide a FE procedure for the implementation in Abaqus/Standard of both MA and FFE applications of the CC, and to offer practical recommendations for their use. In Section 2, the CC theory is recalled. Details on FE implementation of both approaches are described in Section 3. Numerical results are given in section 4.

2. The coupled criterion

In this section, the CC theory is recalled in the case of MA (*cf.* Section 2.1) and FFE (*cf.* Section 2.2) approaches. For the sake of pedagogy, it will only be presented in the bi-dimensional case of an isotropic homogeneous linear elastic material loaded in pure mode I. The MA approach applied to a V-notch in the general mixed mode case is described in the Appendix. As stated in introduction, the CC requires the

simultaneous fulfillment of two separate conditions to ensure crack initiation.

The first condition requires that the stress σ normal to the crack plane overcomes the material tensile strength σ_c on the whole presupposed crack path of length l and described by its arc length parameter s:

$$\sigma(s) \geq \sigma_c \ , \ 0 \leq s \leq l. \tag{1}$$

This stress condition is only a necessary condition for crack initiation. In the case of a monotonically decreasing stress, which is classicaly encountered at singular or stress raisers, the distance l_s on which stress condition is fulfilled increases with increasing imposed loading. Moreover, if the stress condition is satisfied over a distance l_s for a certain imposed loading, it is also verified for all distances l' such that $l' \leq l_s$ (Fig. 1a). Therefore, the stress condition allows determining an upper bound for all the admissible crack lengths at initiation.

The second condition originates from a balance of the kinetic (δW_k), potential (δW_p) and crack surface ($G_c l$, where G_c is the material fracture toughness) energies between the state prior to and after the nucleation of a crack of length l:

$$\delta W_k + \delta W_p + G_c l = 0. \tag{2}$$

A quasi-static initial state implies that $\delta W_k \geq 0$, which allows deriving the energy condition:

$$G^{\text{inc}}(l) = \frac{-\delta W_p}{l} \geq G_c. \tag{3}$$

G^{inc} is called the incremental energy release rate and reverts to the Griffith definition of the energy release

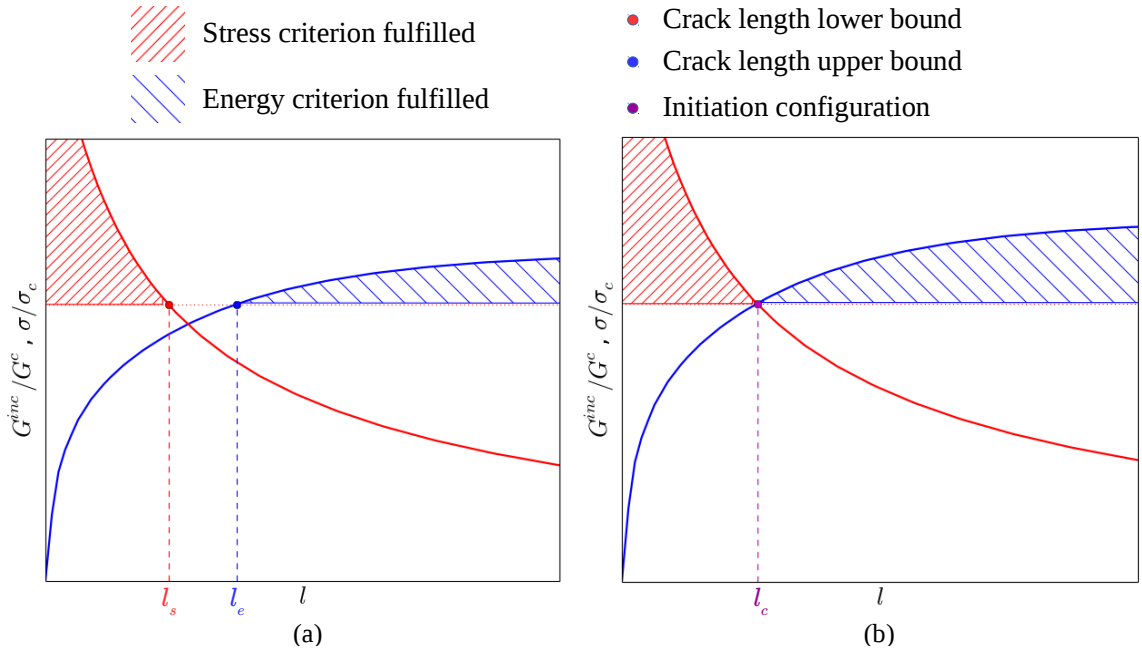

Figure 1: Applied stress to strength ratio $\frac{\sigma}{\sigma_c}$ and incremental energy release rate to fracture toughness ratio $\frac{G^{\text{inc}}}{G_c}$ as a function of the crack length l for a loading (a) lower than the initiation loading (the lower bound of admissible initiation length l_e is higher than the upper bound l_s) and (b) equal to the initiation loading (the lower bound of admissible initiation length l_e is equal to the upper bound l_s and to the initiation length l_c).

rate G when $l \to 0$. Note that G can be expressed as a function of G^{inc} [15, 20, 21, 23], which can be useful to study crack propagation after initiation. However, this point will not be treated in this work which is exclusively dedicated to the prediction of crack initiation. We consider here a positive geometry which implies that the crack propagates in an unstable manner after initiation. This corresponds to a monotonically increasing variation of G^{inc}. Different situations (corresponding to negative geometries for which the crack propagation is stable after initiation) can also be encountered (*cf.* *e.g.*, [15, 19, 23, 28, 32, 33]) . Therefore, for a given imposed loading, if the energy criterion is attained for a crack length l_{e}, it is also attained for all crack lengths l' such that $l' \geq l_{\text{e}}$ (Fig. 1a). The energy condition thus allows determining a lower bound for all the admissible initiation crack lengths. For a too small imposed loading (lower than the initiation loading), the lower bound l_{e} for admissible initiation crack length provided by the energy criterion is higher than the upper bound l_{s} provided by the stress condition hence crack initiation is not possible (*cf.* Fig. 1a). With increasing loading, l_{s} increases whereas l_{e} decreases and the initiation loading and crack length l_{c} can be determined as the loading for which $l_{\text{c}} = l_{\text{e}} = l_{\text{s}}$ which ensures that both the stress and the energy conditions are simultaneously fulfilled (*cf.* Fig. 1b). In the following, as a matter of example, the case of a V-notch specimen (whose dimensions are depicted in Fig. 2) under three-point bending is studied. For the sake of simplicity, a sharp V-notch will be considered. The scripts for the MA and FFE approaches provided as supplementary materials (section 6.4 in the Appendix) also allow to analyze the case of a blunted V-notch [17, 25, 34].

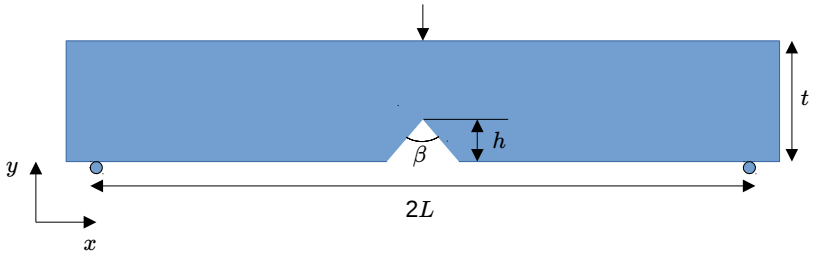

Figure 2: Geometry of the V-notch specimen submitted to three-point bending.

2.1. MA approach

In the example depicted in Fig. 2, a crack initiates at the V-notch in mode I in y-axis direction. In the vicinity of the V-notch tip, under plane elasticity assumption, the outer asymptotic expansion of the far displacement field is given by:

$$\underline{U}(x,y) = \underline{U}(0,0) + kr^{\lambda}\underline{u}(\theta) + ... \tag{4}$$

(x,y) and (r,θ) respectively hold for the cartesian and polar coordinates, $U(0,0)$ denotes the rigid translation of the origin located at the tip of the V-notch, λ is the singularity exponent and $\underline{u}(\theta)$ is an angular shape function. They are solutions to an eigenvalue problem [16] and depend on the V-notch opening angle β. For V-notch opening angles comprised between 0 (crack) and π (straight edge), the exponent λ varies between 0.5 and 1. k is the critical stress intensity factor (GSIF) and is proportional to the applied displacement or load.

The computation of the proportionality factor will be explained at the end of the section and illustrated in Section 3. The application of the CC through the MA approach consists in performing a zoom on a domain surrounding the crack initiation location. Dilating the space variables provides a (theoretically) unbounded domain in which the length of the crack is now equal to 1. This domain is classically denoted as the inner one and is used to define the inner asymptotic expansion of the near field. As shown by previous authors [35], matching the inner expansion (near field) and the outer expansion (far field), the change δW_p in potential energy due to crack initiation over a length l is:

$$-\delta W_p(l) = k^2 l^{2\lambda} B + ..., \tag{5}$$

where B is a geometrical coefficient depending only on the V-notch opening angle β. The energy condition (*cf.* Eq. (3)) then rewrites:

$$G^{\text{inc}} = -\frac{\delta W_p}{l} = k^2 l^{2\lambda-1} B \geq G_{\text{c}}. \tag{6}$$

From Eq. (4) and using an appropriate normalization of the eigenvector $\underline{u}(\theta)$ [10, 34], Eq. (1) rewrites as it is indicated in the Appendix (section 6.1):

$$\sigma(l) = k l^{\lambda-1} \geq \sigma_{\text{c}}. \tag{7}$$

By combining Eqs. (6) and (7), the initiation crack length l_{c} and the critical stress intensity factor k_{c} can be derived:

$$l_{\text{c}} = \frac{G_{\text{c}}}{B\sigma_{\text{c}}^2} = \frac{1}{EB} L_{\text{mat}}, \text{ with } L_{\text{mat}} = \frac{E G_{\text{c}}}{\sigma_{\text{c}}^2}, \tag{8}$$

$$k_{\text{c}} = (\frac{G_{\text{c}}}{B})^{1-\lambda} \sigma_{\text{c}}^{2\lambda-1}. \tag{9}$$

It is worth noting that tabulated values of the coefficient B can be found in a previous paper [34]. The MA approach allows computing the generalized stress intensity factor k_{c} and crack length l_{c} at initiation without considering the whole structure (as depicted, *e.g.*, in Fig 2). Eq. (8) indicates that l_{c} is proportional to the material length L_{mat}. The smallest value is obtained for small opening angles [34] with:

$$l_{\text{c}} \geq l_{\text{c}}^{min} = \frac{L_{\text{mat}}}{2\pi}. \tag{10}$$

Eq. (9) includes the usual Griffith criterion for a crack ($\beta = 0, \lambda = 0.5$) and the strength condition for a straight edge ($\beta = \pi, \lambda = 1$).

The link between the load applied on the structure and the generalized stress intensity factor k^{EF} can be established by computing the following contour integral from a FE analysis on the uncracked structure:

$$k^{\text{EF}} = \frac{\Psi(\underline{U}^{\text{EF}}, r^{-\lambda}\underline{u}^{-}(\theta))}{\Psi(r^{\lambda}\underline{u}(\theta), r^{-\lambda}\underline{u}^{-}(\theta))}, \tag{11}$$

with $\Psi(\underline{U}^{\text{a}}, \underline{U}^{\text{b}}) = \int_{\Gamma} \underline{\underline{\sigma}}(\underline{U}^{\text{a}}) \cdot \underline{N} \cdot \underline{U}^{\text{b}} - \underline{\underline{\sigma}}(\underline{U}^{\text{b}}) \cdot \underline{N} \cdot \underline{U}^{\text{a}} dl$, where Γ is any closed contour surrounding the V-notch and the crack extension and ending on the two faces of the V-notch and $\underline{N}$ the unit normal to Γ pointing toward the V-notch tip. The term $r^{-\lambda}\underline{u}^{-}(\theta)$ is the so-called dual function to the singular mode $r^{\lambda}\underline{u}(\theta)$

[16]. An example of calculation of the stress intensity factor using Eq. (11) is provided as a Supplementary material.

In the case of a blunted V-notch, for which the CC solution is given in Appendix (*cf.* Section 6.3), the inner domain is obtained by dilatation of the coordinates with respect to the blunted V-notch radius d. Hence, contrary to the sharp V-notch for which the crack length in the inner domain is 1 (all quantities being dilated with respect to it), a non-dimensional crack length $\eta = l/d$ is defined.

2.2. FFE approach

In the FFE approach, the whole structure under investigation is considered rather than only a domain surrounding the crack. The stress criterion can thus be computed using only one calculation on the undamaged configuration. Under linear elasticity and the assumption of small deformations, the local stress is proportional to the applied displacement U_0 so that Eq. (1) rewrites:

$$\sigma(s) = \xi(s) E \frac{U_0}{w} \geq \sigma_{\mathrm{c}} \ , \ 0 \leq s \leq l. \tag{12}$$

$\xi(s)$ is a dimensionless function depending only on the structure geometrical features and w a characteristic length of the studied structure (selected here as the sample height as schematised in Fig. 2). Eq. (12) can be rewrited so as to determine the minimum imposed displacement U_0^{stress} necessary to fulfill the stress criterion on a distance l:

$$U_0^{\mathrm{stress}}(l) = w \frac{\sigma_{\mathrm{c}}}{E} \frac{1}{\xi(l)}. \tag{13}$$

The energy criterion requires several calculations with varying crack length in order to compute the potential energy variation, and hence the incremental energy release rate. Under linear elasticity and the assumption of small deformations, the potential energy is proportional to the square applied displacement so that Eq. (3) provides:

$$G^{\mathrm{inc}}(l) = A(l) E w (\frac{U_0}{w})^2 \geq G_{\mathrm{c}}. \tag{14}$$

$A(l)$ is a dimensionless function depending only on the structural geometry. Eq. (14) supplies the minimum imposed displacement U_0^{energy} necessary to fulfill the energy criterion for a crack length l:

$$U_0^{\mathrm{energy}}(l) = w \sqrt{\frac{G_{\mathrm{c}}}{A(l) E w}} = w \frac{\sigma_{\mathrm{c}}}{E} \sqrt{\frac{L_{\mathrm{mat}}}{w}} \frac{1}{\sqrt{A(l)}}, \tag{15}$$

where $\sqrt{\frac{L_{\mathrm{mat}}}{w}}$ is similar to the brittleness number introduced by Mantič [36].

The initiation displacement U^{c} and crack length l_{c} can thus be determined as the minimum applied displacement for which both criteria are fulfilled, *i.e.*:

$$l_{\mathrm{c}} = \underset{l}{\mathrm{argmin}}(max(U_0^{\mathrm{energy}}(l), U_0^{\mathrm{stress}}(l))), \tag{16}$$

$$U^{\mathrm{c}} = max(U_0^{\mathrm{energy}}(l_{\mathrm{c}}), U_0^{\mathrm{stress}}(l_{\mathrm{c}})). \tag{17}$$

In the case of monotonically decreasing stress and monotonically increasing energy release rate, the initiation loading predicted by the stress and the energy conditions are equal so that the initiation length l_{c} can be

estimated by combining and solving Eqs. (13) and (15):

$$\frac{\xi(l_{\rm c})^2}{A(l_{\rm c})} = \frac{\sigma_{\rm c}^2 w}{G_{\rm c} E} = \frac{w}{L_{\rm mat}}. \tag{18}$$

The applied displacement at initiation is then obtained with:

$$\frac{U^{\rm c}}{w\frac{\sigma_{\rm c}}{E}} = \sqrt{\frac{L_{\rm mat}}{w}} \frac{1}{\sqrt{A(l_{\rm c})}} = \frac{1}{\xi(l_{\rm c})}. \tag{19}$$

Eq. (18) reveals that the initiation length $l_{\rm c}$ depends on the material length $L_{\rm mat}$ and on the structural geometry. In the case of a small notch defect submitted to traction, it was shown [31] that the upper bound of the initiation length is:

$$l_{\rm c} \leq l_{\rm c}^{max} = \frac{L_{\rm mat}}{2}. \tag{20}$$

It must be noted that the value of this upper bound was obtained while considering a monotonically increasing behaviour of the incremental energy release rate versus the crack length. Configurations for which $B(l)$ exhibits a maximum are qualified as negative geometries [37]. For these configurations, such as for instance debonding initiation along an interface, $l_{\rm c}^{max}$ is a structural value which only depends on the geometry [19].

3. Finite element procedure - The case of a V-notch specimen

The numerical implementations of the MA and FFE approaches are described in this section, based on the three-point bending geometry depicted in Fig. 2.

3.1. Implementation of the MA approach

The asymptotic approach of the CC requires the coefficient B to be estimated so as to determine the initiation length and stress intensity factor at initiation with the help of Eqs. (8) and (9). The computation of B is based on the potential energy change due to the crack initiation (*cf.* Eq. (6)). The potential energies in presence of and without a crack of length unity are therefore assessed in the inner domain. An example of mesh of the inner domain is presented in Fig. 3. The displacement field related to the V-notch (*cf.* Eq. (4) and Eq. (24) in the Appendix) is imposed as a Dirichlet condition on the domain boundary and the V-notch faces are stress-free. It is recommended to use the exact same mesh topology to compute the potential energy change and to double the node lying on the crack path in the cracked case since it reduces the numerical errors made on the potential energy change. Note that another possibility to calculate the potential energy change consists in using the contour integral Ψ defined by Eq. (11) [18].

The inner domain is artificially bounded at a large distance and boundary conditions are necessary to prescribe a behavior at infinity (matching conditions), thus it is recommended to ensure that the inner domain is large enough. Following the convergence analysis presented in next section, we recommend to use an inner domain radius at least 200 times larger than the largest characteristic length (*e.g.*, crack length, blunt notch radius) in the inner domain. Furthermore, the minimum mesh size $m_{\rm MA}$ at the crack tip must be sufficiently small with $m_{\rm MA} \leq \frac{l}{100}$. The MA procedure also requires that the initiation length remains small compared

to the defect length. Using Eq. (20), which gives an estimate of the upper bound of the initiation length, leads to:

$$L_{\text{mat}} \leq \frac{h}{5}. \tag{21}$$

As will be shown in next section, Eq. (21) must be satisfied to avoid any artefact introduced by the MA approach. In the present example, the stress variation can be derived analytically (Eq. (26) in the Appendix). In other cases for which no analytical solutions exist, it is also possible to compute the stress condition using a FE calculation in the inner domain without crack. It does not require any supplementary calculations than those already performed to compute the potential energy change, but only a post-processing of the FE calculation in the inner domain with no crack. The steps to follow in a FE implementation of the MA approach are the following:

1) Generation of the inner domain geometry and mesh,

2) Computation of the displacement boundary conditions imposed on the inner domain boundary,

3) Computation of the potential energy difference and thus B coefficient, $B = \tilde{W}_{\text{P}}(0) - \tilde{W}_{\text{P}}(1)$ where $\tilde{W}_{\text{P}}$ denotes the potential energy computed in the inner domain and where 0 and 1 denote respectively the uncracked and cracked cases,

4) Introduction of the material properties $(E, \nu, \sigma_{\text{c}}, G_{\text{c}})$ and calculation of the initiation crack length l_{c} and stress intensity factor k_{c} using Eqs. (8) and (9).

It can be noted that the FE calculations in the inner domain can be done once and for all with given values of $(E,\nu)=(E_1,\nu_1)$ for which a value of the coefficient $B = B_1$ is computed. Indeed, it can be shown that the coefficient B_2 corresponding to another couple (E_2,ν_2) can be expressed as a function of B_1 and (E_1, ν_1, E_2, ν_2) with $B_2 = B_1 \frac{1-\nu_2^2}{E_2} \frac{E_1}{1-\nu_1^2}$.

We provide as supplementary data (section 6.4 in the Appendix) a python source code to perform steps 1 to 3 with Abaqus/Standard (ScriptV_notch.py). Standard linear quadratic elements (plane strain conditions)

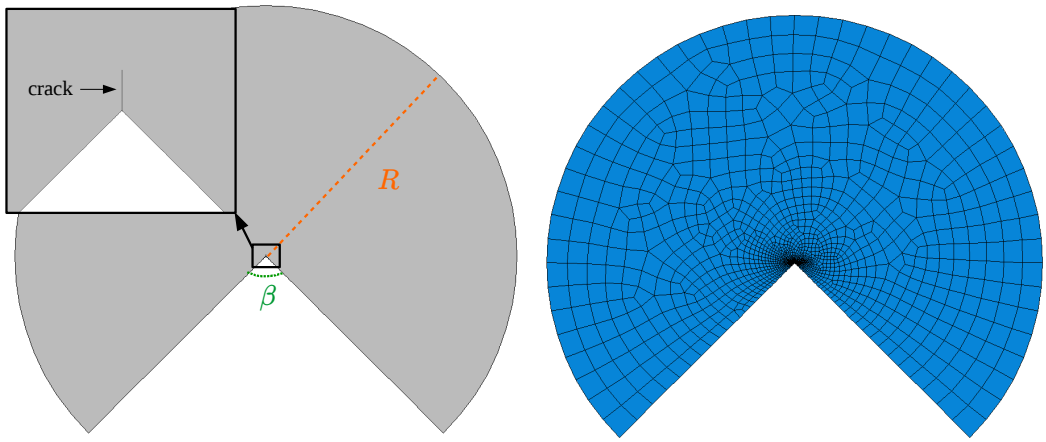

Figure 3: Inner domain of radius R in the case of a V-notch with angle β containing a unity length crack and an example of mesh employed for the computation of the energy difference (MA approach).

are used. Then, a second script solves the CC (step 4) (CC_Solution_from_FE_calculations.py). Those two scripts can also be used to consider a mixed-mode loading. In this case, the crack may initiate with an orientation γ as schematized in Fig. 10. Minimizing $k_{\mathrm{I}}^{c}(\gamma)$ offers an estimate of the initiation angle γ_c. The relevant formulation of the CC is given by Eqs. (31) and (32) in section 6.2 of the Appendix. The calculations for several V-notch openings β and crack angles γ have been performed (with E= 1 MPa and ν=0.36) and the results were stored in a database file (Data_Vnotch_r0.txt) provided as a Supplementary material. Similar results (only with $\gamma = 0$) were already given in a previous paper [34]. A python script (Solution_Vnotch_r0_modeIandII.py) allows solving the CC (step 4) in the case of a sharp V-notch (under mode I and mixed mode loading) using the MA without any FE calculations. It only requires these pre-calculated data and is therefore computationally very efficient.

Eqs. (43) and (44) in Section 6.3 of the Appendix give the formulation of the CC for a blunt V-notch under mixed-mode loading. The same scripts (ScriptV_notch.py) and (CC_Solution_from_FE_calculations.py) can be used to solve the CC with the MA approach. As already mentioned, the inner domain is obtained by dilatation of the spatial coordinates with respect to the blunted V-notch radius d and a non-dimensional crack length $\eta = l/d$ is introduced. Therefore, an estimate of an upper bound to the initiation crack length must be obtained before generating the FE mesh of the inner domain including a blunted V-notch radius of dimension 1 and a crack of non dimensional length η. In practice, the following procedure must be followed so as to compute the maximum non-dimensionnal crack length in the inner domain:

1) Choose the minimum blunted V-notch radius $d_{\min}$ for which the CC solution has to be calculated,

2) Estimate the maximum initiation length with the condition $l_{\mathrm{c}} \leq \frac{L_{\mathrm{mat}}}{2}$,

3) Compute the non-dimensional upper bound for the initiation length $\frac{L_{\mathrm{mat}}}{2d_{\min}}$ that can be employed to generate the inner domain mesh.

Then the MA approach can be used as already described in Section 2.1.

3.2. Implementation of the FFE approach

Crack initiation length l_{c} and loading level U^{c} are determined using Eqs. (18) and (19), which involves the dimensionless functions $A(l)$ and $\xi(s)$. The computation of ξ only requires one calculation on the structure without crack, whereas several calculations with increasing crack lengths are requested so as to obtain A. Similarly to the MA approach, it is recommended to use the exact same mesh topology to compute the potential energy change by successively releasing the nodes lying on the crack path. A refined mesh of length M_{FFE} with the mesh size m_{FFE} (Fig. 4) must be introduced in the vicinity of the notch in order to capture accurately the initiation length l_{c}. Using the lower bound l_{c}^{min} defined by Eq. (10) and the upper bound l_{c}^{max} defined by Eq. (20), a convergence analysis presented in next section leads to select:

$$m_{\mathrm{FFE}} \leq \frac{l_{\mathrm{c}}^{min}}{6} = \frac{L_{\mathrm{mat}}}{12\pi}, \tag{22}$$

$$M_{\mathrm{FFE}} \geq l_{\mathrm{c}}^{max} = \frac{L_{\mathrm{mat}}}{2}. \tag{23}$$

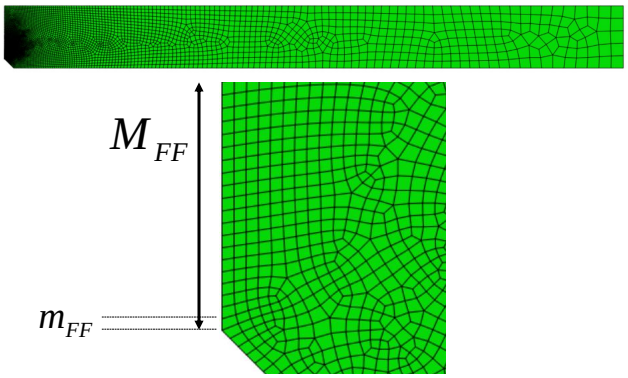

Figure 4: Refined mesh at the V-notch tip (FFE approach): the minimum mesh size and the length of the refined zone are respectively denoted m_{FFE} and M_{FFE}.

If the node distribution is regular, the number of calculations necessary to evaluate the incremental energy release rate A is $N \geq \frac{M_{\mathrm{FFE}}}{m_{\mathrm{FFE}}} = 6\pi \cong 20$. It will be shown in next section that N can be reduced by introducing a controlled variation of the mesh size within the refined zone. The steps to follow for a FE implemention of the FFE approach are the following:

1) Generation of the geometry and mesh of the studied structure,

2) Generation of several meshes with varying crack length,

3) Introduction of the material properties (E, ν) and computation of the scale factors ξ and A,

4) Introduction of the material properties $(\sigma_{\mathrm{c}}, G_{\mathrm{c}})$ and calculation of the initiation crack length and loading level using Eqs. (18) and (19).

In practice, the dimensionless functions ξ and A do not depend on Young's modulus E and reveal weakly dependant on Poisson's ratio ν so that the material properties are only needed for the last step. We provide as supplementary data (section 6.4 in the Appendix) a python source code (F3P_Vnotch.py) for steps 1 to 3 (using Abaqus/Standard) and a complementary one (post_F3P.py) for step 4. Standard linear quadratic elements (plane strain conditions) are still used.

4. Numerical results

This section includes several convergence analysis and a comparison between MA and FFE approaches.

4.1. Convergence analysis to estimate the minimum mesh size and the radius of the inner domain (MA approach)

Convergence analyses are performed in order to determine the best meshing conditions of the inner domain. Fig. 5 shows the influence of the minimum mesh m_{MA} size at the crack tip to crack length l ratio on the coefficient B. The condition $\frac{m_{\mathrm{MA}}}{l} \leq 0.01$ must be satisfied to reach convergence. The effect of the radius R of the inner domain on the initiation stress intensity factor and crack length is depicted on Fig. 6.

Both quantities are overestimated using a too small inner domain radius and converge to a constant value for larger domain radii with $R \geq 200\ l$. It is thus recommanded to keep the radius of the inner domain 200 times larger than the largest characteristic length.

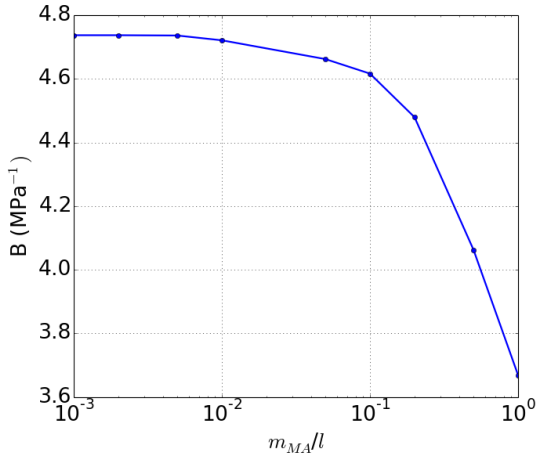

Figure 5: Coefficient B (MA approach) versus the minimum mesh size to crack length ratio $\frac{m_{\mathrm{MA}}}{l}$ for a sharp V-Notch with $\beta = 90$deg., $E = 3300$MPa , ν =0.36. The inner domain radius to crack length ratio is $\frac{R}{l}$=200.

4.2. Convergence analysis to estimate the minimum mesh size (FFE approach)

Fig. 7 depicts the crack length and applied displacement at initiation versus the ratio $\frac{L_{\mathrm{mat}}}{w}$ for given values of h and β. For large values of the minimum mesh size, l_{c} and U^{c} are overestimated but decreasing m_{FFE} towards the reference value m^{REF}=0.5 µm clearly demonstrates a convergence. Fig. 8a shows that a value $m_{\mathrm{FFE}} \leq 1\ \mu$m is necessary to maintain the relative error with the reference solution below 1%. Similar

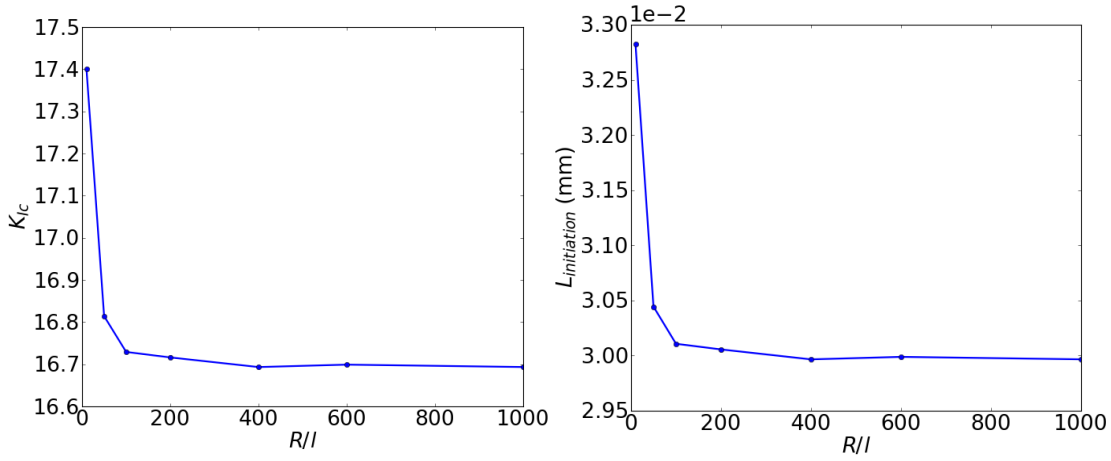

Figure 6: Initiation (a) critical stress intensity factor and (b) crack length determined with the MA approach as a function of the inner domain radius to crack length ratio for a sharp V-Notch with $\beta = 90$deg., $E = 3300$MPa , ν =0.36 , σ_{c} =72MPa and G_{c} =0.250MPa.mm. The minimum mesh size to crack length ratio is $\frac{m_{\mathrm{MA}}}{l}$=0.01.

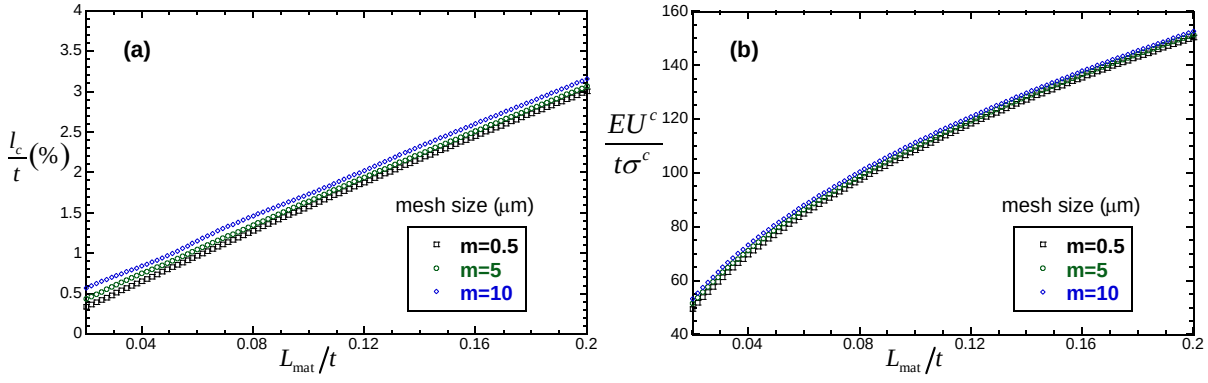

Figure 7: a) Initiation length and b) Applied displacement determined with the FFE approach versus the characteristic length for different values of the minimum mesh size m_{FFE} at the notch tip with M_{FFE} =200μm. The three-point bending geometry with a sharp V-notch is considered with $2L = 40$mm, $w = 2$mm, $h = 0.3$mm, $\beta = 40$deg. and E=400 GPa, $\nu = 0.2$.

results were obtained for another angles β and V-notch depth h, which leads to recommand a mesh size $m_{\mathrm{FFE}} \leq \frac{l_c^{min}}{6} = \frac{L_{\mathrm{mat}}}{12\pi}$. Employing a non-uniform mesh is useful to reduce the number of nodes within the refined zone. This is illustrated in Fig. 8b: starting from a mesh size m_{FFE}=1.5 μm, a bias is introduced in order to verify the condition (22) close to the notch tip while allowing progressively a larger mesh size away from the notch tip. This procedure does not degrade or improve the accuracy but allows to reduce the number of calculations required to evaluate the scale factor A.

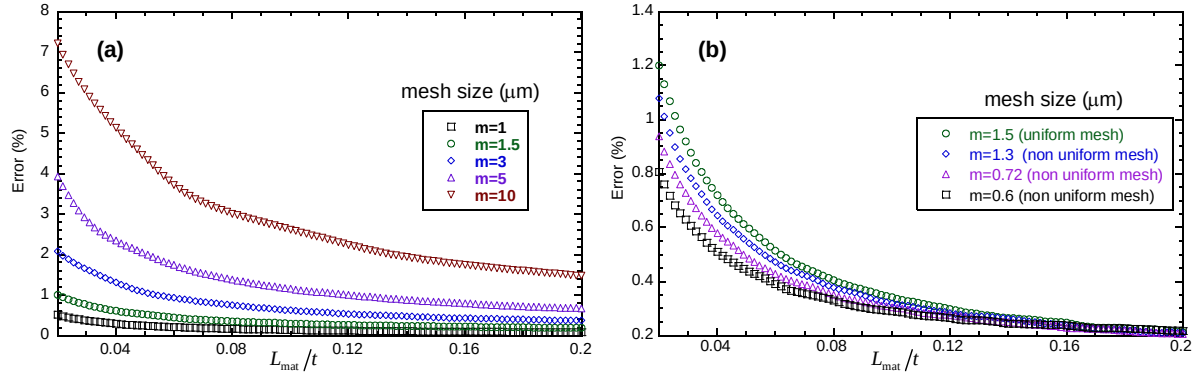

Figure 8: Relative error $\frac{U^c(m_{\mathrm{FFE}})-U^c(m^{REF})}{U^c(m^{REF})}$ in terms of applied displacement at initiation versus the characteristic length (FFE approach) m^{REF} =0.5 μm : a) The mesh is uniform, b) The mesh is non-uniform and obtained after introducing a bias. The three-point bending geometry with a sharp V-notch is analysed with $2L = 40$ mm, $w = 2$ mm, $h = 0.3$ mm, $\beta = 40$deg. and E=400 GPa, $\nu = 0.2$ and M_{FFE} =200μm.

4.3. Comparison between MA and FFE approaches

MA and FFE approaches are now used to estimate the influence of the V-notch angle on crack initiation for the three-point bending geometry (Fig. 2) with $2L = 40$ mm, $w = 2$ mm and $h = 0.3$ mm. The minimum mesh size and the radius of the inner domain employed with the MA method are respectively m_{MA} =10μm

and R=200mm with l=1mm. The minimum mesh size and the length of the refined zone employed with the FFE method are respectively $m_{\mathrm{FFE}} = m^{\mathrm{REF}}$ =0.5 μm and M_{FFE} =200 μm. The MA approach requires the calculation of the GSIF for a given applied displacement with the contour integral defined by Eq. (11) (which can be obtained using the script Compute_K2D.py provided in supplementary materials). Results displayed in Fig. 9a show that the applied critical displacement increases with the notch angle. Both procedures give similar results for lower values of the characteristic length but a significant difference appears with increasing L_{mat}. The explanation is provided by Fig. 9b which plots the initiation length at crack initiation versus the notch angle: l_{c} increases with L_{mat} and β. As the scaling factor linking l_{c} and L_{mat} reveals smaller for the FF approach for higher values of L_{mat}, smaller initiation lengths are estimated with the FF method for larger values of L_{mat}. To remain within the framework of the asymptotic analysis, the initiation length must be at least one order of magnitude smaller than the notch length with $l_{\mathrm{c}} \leq \frac{h}{10}$=30 μm. This condition is no more satisfied for every notch angle for increasing values of L_{mat} for which the MA results exhibits (in Fig. 9a) a non-physical minimum corresponding to a "critical angle" as already shown by previous authors [38].

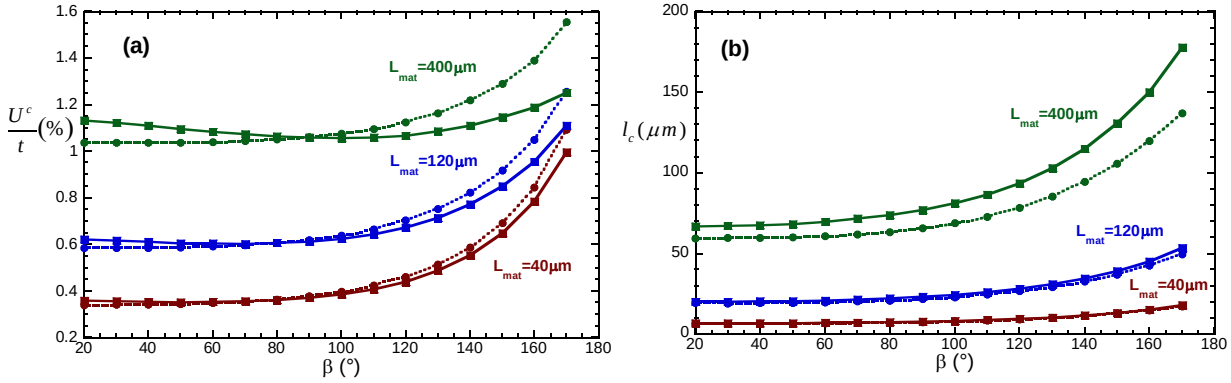

Figure 9: Comparison between MA (square symbols and full lines) and FFE (disk symbols and dotted lines) approaches: a) Applied displacement and b) Initiation length at crack onset versus the notch angle for various values of the characteristic length L_{mat}. A three-point bending specimen with a sharp V-notch is considered with $2L$ = 40 mm, w = 2 mm, h = 0.3 mm and E=400 GPa, ν = 0.2, σ^c = 100 MPa and Gc=1, 3 or 10 J/m^2 corresponding to Lmat=40, 120, or 400 μm.

5. Conclusion

To predict crack initiation in the vicinity of a stress concentration, the CC can be implemented with the help of MA or FFE methods. Both procedures are detailed in this paper in order to facilitate their use with a FE code. In addition, python source codes are provided to illustrate their implementation in Abaqus/Standard in the case of a sharp or a blunted V-notch. The supplied tools apply the MA approach for mixed mode loading and the FFE approach for a specimen submitted to three-point bending. Results of convergence analysis are analysed to link the characteristic length of the studied material with the needed mesh refinement at the notch tip for the FFE method. The MA approach allows the initiation loading and crack length to be determined without considering the whole structure under investigation by performing a

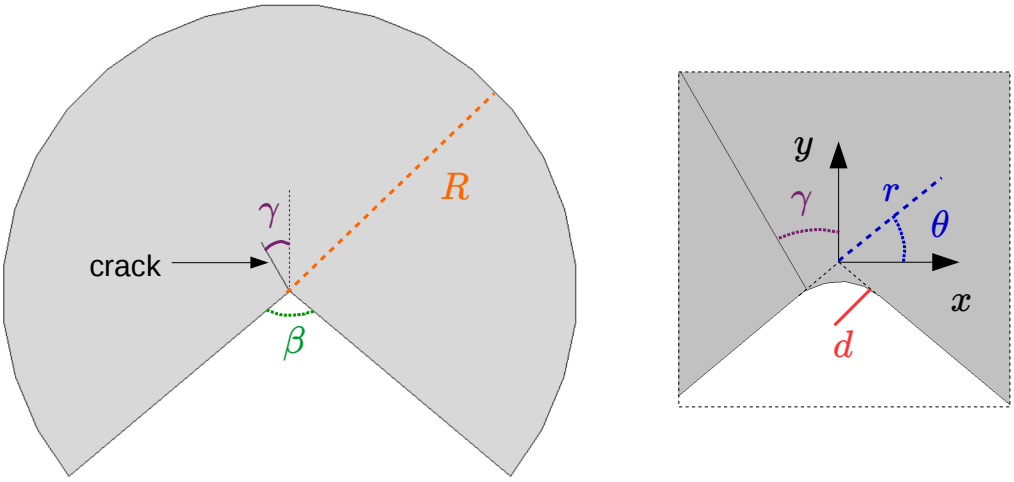

Figure 10: Inner domain of radius R containing a V-notch with opening angle β and tip radius d and a crack oriented with an angle γ with respect to Oy axis.

zoom around the crack initiation location. It is computationally more efficient than the FFE approach that requires several calculations with different crack lengths to be computed on the whole model. The domain in which the calculations are performed must be large enough to prescribe a behavior "at infinity" (see Section 3.1). The asymptotic approach is restricted by the assumption that the initiation length is small compared to the structure characteristic dimensions, and that the crack location is far enough from any boundary or features that may affect the displacement/stress field around the crack. If these assumptions are not fulfilled, some differences on initiation crack length and loading level are obtained between both approaches. This is directly linked to the material characteristic length L_{mat} which has an influence on the predicted initiation length (that also depends on the geometrical features of the studied structure). An additional study is needed to quantify more precisely these differences, nevertheless condition (21) provides a validity range estimate for the MA approach.

6. Appendix

The CC solution in mixed mode using the asymptotic approach is explained in this appendix for either sharp or blunted V-notch, which of course includes the particular case of a sharp V-notch specimen loaded under pure mode I loading presented in the paper for the sake of pedagoy. The scripts provided as supplementary data allow studying general cases of blunted V-notch under mixed mode loading.

6.1. Singularity exponents and asymptotic displacement field

The displacements in the vicinity of a traction free V-notch can be expressed by an asymptotic series, for which the first three terms expressed in polar coordinates are:

$$u(r,\theta) = \left\{ \begin{array}{c} u_r \\ u_\theta \end{array} \right\} = \mathbf{u}(0,0) + k_{\text{I}} r^{\lambda_1} \left\{ \begin{array}{c} u_r^I(\theta) \\ u_\theta^I(\theta) \end{array} \right\} + k_{\text{II}} r^{\lambda_2} \left\{ \begin{array}{c} u_r^{II}(\theta) \\ u_\theta^{II}(\theta) \end{array} \right\} \tag{24}$$

with

$u_r^I(\theta) = [cos((1+\lambda_1)\theta^*) + \frac{\lambda_L+3\mu_L-\lambda_1(\lambda_L+\mu_L)}{(\lambda_L+\mu_L)(1-\lambda_1)} \frac{sin(\omega(1+\lambda_1)/2)}{sin(\omega)(1-\lambda_1)/2)} cos((1-\lambda_1)\theta^*)]/(2\mu_L\lambda_1\sigma_{\theta\theta}^{I-0})$

$u_\theta^I(\theta) = [-sin((1+\lambda_1)\theta^*) - \frac{\lambda_L+3\mu_L+\lambda_1(\lambda_L+\mu_L)}{(\lambda_L+\mu_L)(1-\lambda_1)} \frac{sin(\omega(1+\lambda_1)/2)}{sin(\omega)(1-\lambda_1)/2)} sin((1-\lambda_1)\theta^*)]/(2\mu_L\lambda_1\sigma_{\theta\theta}^{I-0})$

$u_r^{II}(\theta) = [sin((1+\lambda_2)\theta^*) + \frac{\lambda_L+3\mu_L-\lambda_2(\lambda_L+\mu_L)}{(\lambda_L+\mu_L)(1+\lambda_2)} \frac{sin(\omega(1+\lambda_2)/2)}{sin(\omega)(1-\lambda_2)/2)} sin((1-\lambda_2)\theta^*)]/(2\mu_L\lambda_2\sigma_{r\theta}^{II-0})$

$u_\theta^{II}(\theta) = [cos((1+\lambda_2)\theta^*) + \frac{\lambda_L+3\mu_L+\lambda_2(\lambda_L+\mu_L)}{(\lambda_L+\mu_L)(1+\lambda_2)} \frac{sin(\omega(1+\lambda_2)/2)}{sin(\omega)(1-\lambda_2)/2)} cos((1-\lambda_2)\theta^*)]/(2\mu_L\lambda_2\sigma_{r\theta}^{II-0})$

where λ_L, μ_L are the Lamé coefficient, $\theta^* = \theta - \pi/2$, $\omega = 2\pi - \beta$ and

$\sigma_{\theta\theta}^{I-0} = \frac{(1+\lambda_1)sin(\omega(1+\lambda_1)/2)}{(1-\lambda_1)sin(\omega(1-\lambda_1)/2)} - 1$

$\sigma_{r\theta}^{II-0} = 1 - \frac{(1-\lambda_2)sin(\omega(1+\lambda_2)/2)}{(1+\lambda_2)sin(\omega(1-\lambda_2)/2)}$

The singularity exponents λ_1 and λ_2 associated with a V-notch with opening angle β can be computed as the smallest roots of the following characteristic equations:

$$\begin{cases} sin(\lambda_1(2\pi-\beta)) + \lambda_1 sin(2\pi-\beta) = 0 \\ sin(\lambda_2(2\pi-\beta)) - \lambda_2 sin(2\pi-\beta) = 0 \end{cases} \tag{25}$$

The stress field in the vicinity of the V-notch can be expressed in polar coordinates as:

$$\sigma(r,\theta) = \begin{Bmatrix} \sigma_{rr} \\ \sigma_{\theta\theta} \\ \sigma_{r\theta} \end{Bmatrix} = k_I r^{\lambda_1-1} \begin{Bmatrix} \sigma_{rr}^I(\theta) \\ \sigma_{\theta\theta}^I(\theta) \\ \sigma_{r\theta}^I(\theta) \end{Bmatrix} + k_{II} r^{\lambda_2-1} \begin{Bmatrix} \sigma_{rr}^{II}(\theta) \\ \sigma_{\theta\theta}^{II}(\theta) \\ \sigma_{r\theta}^{II}(\theta) \end{Bmatrix} \tag{26}$$

with

$\sigma_{rr}^I(\theta) = [cos((1+\lambda_1)\theta^*) + \frac{3-\lambda_1}{1-\lambda_1} \frac{sin(\omega(1+\lambda_1)/2)}{sin(\omega)(1-\lambda_1)/2)} cos((1-\lambda_1)\theta^*)]/\sigma_{\theta\theta}^{I-0}$

$\sigma_{\theta\theta}^I(\theta) = [-cos((1+\lambda_1)\theta^*) + \frac{1+\lambda_1}{1-\lambda_1} \frac{sin(\omega(1+\lambda_1)/2)}{sin(\omega(1-\lambda_1)/2)} cos((1-\lambda_1)\theta^*)]/\sigma_{\theta\theta}^{I-0}$

$\sigma_{r\theta}^I(\theta) = [-sin((1+\lambda_1)\theta^*) + \frac{sin(\omega(1+\lambda_1)/2)}{sin(\omega(1-\lambda_1)/2)} sin((1-\lambda_1)\theta^*)]/\sigma_{\theta\theta}^{I-0}$

$\sigma_{rr}^{II}(\theta) = [sin((1+\lambda_2)\theta^*) + \frac{3-\lambda_2}{1+\lambda_2} \frac{sin(\omega(1+\lambda_2)/2)}{sin(\omega(1-\lambda_2)/2)} sin((1-\lambda_2)\theta^*)]/\sigma_{\theta\theta}^{II-0}$

$\sigma_{\theta\theta}^{II}(\theta) = [-sin((1+\lambda_2)\theta^*) + \frac{sin(\omega(1+\lambda_2)/2)}{sin(\omega(1-\lambda_2)/2)} sin((1-\lambda_1)\theta^*)]/\sigma_{\theta\theta}^{II-0}$

$\sigma_{r\theta}^{II}(\theta) = [cos((1+\lambda_2)\theta^*) - \frac{1-\lambda_2}{1+\lambda_2} \frac{sin(\omega(1+\lambda_2)/2)}{sin(\omega(1-\lambda_2)/2)} cos((1-\lambda_2)\theta^*)]/\sigma_{r\theta}^{II-0}$

6.2. The sharp V-notch under mixed mode loading

In the context of matched asymptotic expansions, the inner domain is dilated with respect to the crack length l. In this case the potential energy difference for a V-notch with opening angle β is expressed as:

$$\begin{cases} -\delta W_p = k_I^2 l^{2\lambda_1}(B_{11}(\gamma) + m(l)B_{12}(\gamma) + m(l)^2 B_{22}(\gamma)) \\ m(l) = \frac{k_{II}}{k_I} l^{\lambda_2-\lambda_1} \end{cases} \tag{27}$$

where γ defines the crack angle with respect to the V-notch bisector (Fig. 10). Therefore the energy condition of the CC writes:

$$G^{inc} = -\frac{\delta W_p}{l} = k_I^2 l^{2\lambda_1-1}(B_{11}(\gamma) + m(l)B_{12}(\gamma) + m(l)^2 B_{22}(\gamma)) \geqslant G_c \tag{28}$$

The stress condition of the CC writes:

$$\sigma_{\theta\theta} = k_I l^{\lambda_1-1}(\sigma_{\theta\theta}^I(\gamma) + m(l)\sigma_{\theta\theta}^{II}(\gamma)) \geqslant \sigma_c \tag{29}$$

Therefore, the generalized stress intensity factor k_{I} can be computed by combining Eqs. (28) and (29):

$$k_{\mathrm{I}} = \left(\frac{G_c}{B_{11}(\gamma) + m(l)B_{12}(\gamma) + m(l)^2 B_{22}(\gamma)}\right)^{1-\lambda_1} \left(\frac{\sigma^I_{\theta\theta}(\gamma) + m(l)\sigma^{II}_{\theta\theta}(\gamma)}{\sigma_c}\right)^{1-2\lambda_1} \tag{30}$$

Using Eq. (28), the initiation crack length l_c can be obtained by solving the following equation which is implicit because m depends on l_c:

$$l_c = \frac{G_c}{B_{11}(\gamma) + m(l_c)B_{12}(\gamma) + m(l_c)^2 B_{22}(\gamma)} \left(\frac{\sigma^I_{\theta\theta}(\gamma) + m(l_c)\sigma^{II}_{\theta\theta}(\gamma)}{\sigma_c}\right)^2 \tag{31}$$

which allows determining the critical GSIF k^c_{I}

$$k^c_{\mathrm{I}} = \left(\frac{G_c}{B_{11}(\gamma) + m(l_c)B_{12}(\gamma) + m(l_c)^2 B_{22}(\gamma)}\right)^{1-\lambda_1} \left(\frac{\sigma_c}{\sigma^I_{\theta\theta}(\gamma) + m(l_c)\sigma^{II}_{\theta\theta}(\gamma)}\right)^{2\lambda_1-1} \tag{32}$$

For a given V-notch opening angle β, the critical GSIF is estimated for several crack angles γ, the initiation GSIF and crack angle being given by the configuration minimizing k^c_{I}. In practice, the solution of the CC requires the knowledge of the functions B_{ij} (i,j=1 or 2) and $\sigma^k_{\theta\theta}$ (k=I or II). The latter can be computed analytically in the case of a sharp V-notch (*cf.* Eq. (26)) while the former have to be computed by FE computations. First, FE calculations are performed for (k_{I}=1, k_{II}=0) in order to estimate the potential energies with ($\delta W^{\mathrm{I}}_{\mathrm{p}}(l)$) and without ($\delta W^{\mathrm{I}}_{\mathrm{p}}(0)$) a crack in pure mode I (and hence their difference $-\delta W^{\mathrm{I}}_{\mathrm{p}}$=$\delta W^{\mathrm{I}}_{\mathrm{p}}(0) - \delta W^{\mathrm{I}}_{\mathrm{p}}(l)$) from the stress σ^I and strain ϵ^I fields.

$$\delta W^{\mathrm{I}}_{\mathrm{p}} = \frac{1}{2}\int_\Omega \underline{\underline{\sigma}}^I : \underline{\underline{\epsilon}}^I dV \tag{33}$$

It provides B_{11} for a given crack angle γ (the procedure being repeted for crack angles γ varying between -90 and 0 deg.), from Eq. (27):

$$B_{11}(\gamma) = \frac{-\delta W^{\mathrm{I}}_{\mathrm{p}}}{k^2_{\mathrm{I}} l^{2\lambda_1}} = \delta W^{\mathrm{I}}_{\mathrm{p}}(0) - \delta W^{\mathrm{I}}_{\mathrm{p}}(l) \text{ since } k_{\mathrm{I}} = 1 \text{ and } l = 1 \tag{34}$$

Then, FE calculations are performed for (k_{I}=0, k_{II}=1) in order to evaluate the potential energies with ($\delta W^{\mathrm{II}}_{\mathrm{p}}(l)$) and without ($\delta W^{\mathrm{II}}_{\mathrm{p}}(0)$) a crack in pure mode II (and hence their difference $-\delta W^{\mathrm{II}}_{\mathrm{p}}$=$\delta W^{\mathrm{II}}_{\mathrm{p}}(0) - \delta W^{\mathrm{II}}_{\mathrm{p}}(l)$) from the stress σ^{II} and strain ϵ^{II} fields.

$$\delta W^{\mathrm{II}}_{\mathrm{p}} = \frac{1}{2}\int_\Omega \underline{\underline{\sigma}}^{II} : \underline{\underline{\epsilon}}^{II} dV \tag{35}$$

It allows determining A_{22} for a given crack angle γ (the procedure being repeted for crack angles γ varying between -90 and 0 deg.), from Eq. (27):

$$B_{22}(\gamma) = \frac{-\delta W^{\mathrm{II}}_{\mathrm{p}}}{k^2_{\mathrm{II}} l^{2\lambda_2}} = \delta W^{\mathrm{II}}_{\mathrm{p}}(0) - \delta W^{\mathrm{II}}_{\mathrm{p}}(l) \text{ since } k_{\mathrm{II}} = 1 \text{ and } l = 1 \tag{36}$$

Finally, the knowledge of B_{11} and B_{22} gives access to B_{12} by computing the potential energy difference $-\delta W^{\mathrm{I+II}}_{\mathrm{p}}$ for any GSIFs so that (k_{I},k_{II})$\neq$(0,0). For the sake of simplicity, we choose (k_{I}=1, k_{II}=1).

$$B_{12}(\gamma) = \frac{1}{m(l)}\left(\frac{-\delta W^{\mathrm{I+II}}_{\mathrm{p}}}{k^2_{\mathrm{I}} l^{2\lambda_1}} - A_{11}(\gamma) - m(l)^2 A_{22}(\gamma)\right) \tag{37}$$

Actually, no extra FE calculations than those in pure mode I and pure mode II are required to compute B_{12} since the potential energy in mode I+II can be computed by combining the stress and strain fields obtained in pure mode I and II:

$$\delta W_{\mathrm{p}}^{\mathrm{I+II}} = \frac{1}{2}\int_{\Omega} (\underline{\underline{\sigma}}^{I} + \underline{\underline{\sigma}}^{II}) : (\underline{\underline{\epsilon}}^{I} + \underline{\underline{\epsilon}}^{II}) dV \tag{38}$$

hence simplifying Eq. (37) into:

$$B_{12}(\gamma) = -\delta W_{\mathrm{p}}^{\mathrm{I+II}} - B_{11}(\gamma) - B_{22}(\gamma) \text{ since } k_{\mathrm{I}} = 1, k_{\mathrm{II}} = 1 \text{ and } l = 1 \tag{39}$$

6.3. The blunted V-notch under mixed mode loading

In the case of a V-notch with a blunted tip of radius d (*cf.* Fig. 10), the inner domain is dilated with respect to either the crack length l or the notch radius d (leading to the same results). For practical reasons (ease of FE mesh generation), we choose a dilatation with respect to d hence defining the normalized crack length $\eta = l/d$. The potential energy difference reads:

$$\begin{cases} -\delta W_{\mathrm{p}} = k_{\mathrm{I}}^2 d^{2\lambda_1}(B_{11}^b(\gamma,\eta) + m(d)B_{12}^b(\gamma,\eta) + m(d)^2 B_{22}^b(\gamma,\eta)) \\ m(d) = \frac{k_{\mathrm{II}}}{k_{\mathrm{I}}} d^{\lambda_2 - \lambda_1} \end{cases} \tag{40}$$

Therefore the energy condition of the CC writes:

$$G^{inc} = -\frac{\delta W_{\mathrm{p}}}{l} = k_{\mathrm{I}}^2 l^{2\lambda_1 - 1} \frac{B_{11}^b(\gamma,\eta) + m(d)B_{12}^b(\gamma,\eta) + m(d)^2 B_{22}^b(\gamma,\eta)}{\eta^{2\lambda_1}} \geqslant G_c \tag{41}$$

The stress condition of the CC writes:

$$\sigma_{\theta\theta} = k_{\mathrm{I}} d^{\lambda_1 - 1}(\sigma_{\theta\theta}^{Ib}(\gamma,\eta) + m(d)\sigma_{\theta\theta}^{IIb}(\gamma,\eta)) \geqslant \sigma_c \tag{42}$$

where $\sigma_{\theta\theta}^{kb}$ differs from $\sigma_{\theta\theta}^{k}$ ($k = I$ or II) defined in Section 6.2 because of the blunted notch tip. These functions can be computed by FE calculations on uncracked configuration. By combining Eqs. (41) and (42), we obtain the equation that must be solved so as to determine the initiation crack length $l_c = d\eta_c$ for a given value of γ:

$$\frac{1}{(\sigma_{\theta\theta}^{Ib}(\gamma,\eta) + m(d)\sigma_{\theta\theta}^{IIb}(\gamma,\eta))^2} \frac{B_{11}^b(\gamma,\eta_c) + m(d)B_{12}^b(\gamma,\eta_c) + m(d)^2 B_{22}^b(\gamma,\eta_c)}{\eta_c} = \frac{1}{d}\frac{G_c}{\sigma_c^2} \tag{43}$$

It can be noted that the solution of Eq. (43) depends on the actual value of the the blunted notch radius d (expressed in length unit) and not on a ratio between d and another characteristic length. From (41) and (42) we deduce the critical GSIF:

$$k_{\mathrm{I}}^c = \left(\frac{G_c}{D(\gamma,\eta_c)}\right)^{1-\lambda_1} \left(\frac{\sigma_c}{\sigma_{\theta\theta}^{Ib}(\gamma,\eta_c) + m(d)\sigma_{\theta\theta}^{IIb}(\gamma,\eta_c)}\right)^{2\lambda_1 - 1} \tag{44}$$

with $D(\gamma,\eta_c) = \frac{B_{11}^b(\gamma,\eta_c) + m(d)B_{12}^b(\gamma,\eta_c) + m(d)^2 B_{22}^b(\gamma,\eta_c)}{\eta_c}$

The crack initiation angle γ_c is solved as the one minimizing the critical GSIF k_{I}^c. In practice, the solution of the CC for the blunted V-notch requires the knowledge of the functions B_{ij}^b (i,j=1 or 2) and $\sigma_{\theta\theta}^K b$ (k=I or II). Contrary to the sharp V-notch case, the latter are not computed analytically but by means of FE calculations, as well as the former. For a given V-notch opening, B_{ij}^b must be computed for several crack

angles γ and normalized lengths η_c in order to solve Eq. (43) for all these angles and find the one minimizing k_{I}^c. In fact, it was shown in [25] that the same crack initiation angle as for a sharp V-notch was found for a blunted V-notch. Therefore, the computation of B_{ij}^b can directly be performed for the crack angle γ_c that minimizes the GSIF in the case of a sharp V-notch, which reduces the number of calculations required to solve the CC. The same approach as described in Section 6.2 is adopted to compute the B_{ij}^b functions.

6.4. Supplementary data

Supplementary data associated with this article can be found in the online version. Scripts to be used with Abaqus/Standard are provided for the MA approach (Script_V_notch.py, Auxiliary_functions.py, CC_Solution_from_FE_calculation.py, Data_Vnotch_r0.txt and Solution_Vnotch_r0_modeIandII.py, Compute_K2D.py) and for the FFE approach (F3P_Vnotch.py and post_F3P.py) together with the corresponding instruction files (Readme_MA.txt and Readme_FFE.txt).

References

[1] G. Barenblatt, The formation of equilibrium cracks during brittle fracture. General ideas and hypotheses. Axially-symmetric cracks, Journal of Applied Mathematics and Mechanics. 23 (1959) 622636.

[2] D.S. Dugdale, Yielding of steel sheets containing slits, Journal of the Mechanics and Physics of Solids. 8 (1960) 100104.

[3] V. Tvergaard, J.W. Hutchinson, The relation between crack growth resistance and fracture process parameters in elastic-plastic solids, Journal of the Mechanics and Physics of Solids. 40 (1992) 13771397. doi:10.1016/0022-5096(92)90020-3.

[4] X.-P. Xu, A. Needleman, Numerical simulations of fast crack growth in brittle solids, Journal of the Mechanics and Physics of Solids. 42 (1994) 13971434. doi:10.1016/0022-5096(94)90003-5.

[5] C. Giry, F. Dufour, J. Mazars, Stress-based nonlocal damage model, International Journal of Solids and Structures. 48 (2011) 34313443. doi:10.1016/j.ijsolstr.2011.08.012.

[6] G. Pijaudier-Cabot, Z.P. Bažant, Nonlocal Damage Theory, Journal of Engineering Mechanics. 113 (1987) 15121533. doi:10.1061/(ASCE)0733-9399(1987)113:10(1512).

[7] B. Bourdin, G.A. Francfort, J.-J. Marigo, Numerical experiments in revisited brittle fracture, Journal of the Mechanics and Physics of Solids. 48 (2000) 797826. doi:10.1016/S0022-5096(99)00028-9

[8] C. Miehe, F. Welschinger, M. Hofacker, Thermodynamically consistent phase-field models of fracture: Variational principles and multi-field FE implementations, Int. J. Numer. Meth. Engng. 83 (2010) 12731311. doi:10.1002/nme.2861.

[9] G. Molnár, A. Gravouil, 2D and 3D Abaqus implementation of a robust staggered phase-field solution for modeling brittle fracture, Finite Elements in Analysis and Design. 130 (2017) 2738. doi:10.1016/j.finel.2017.03.002.

[10] D. Leguillon, Strength or toughness? A criterion for crack onset at a notch, European Journal of Mechanics - A/Solids. 21 (2002) 6172. doi:10.1016/S0997-7538(01)01184-6.

[11] A. Carpinteri, P. Cornetti, N. Pugno, A. Sapora, D. Taylor, A finite fracture mechanics approach to structures with sharp V-notches, Engineering Fracture Mechanics. 75 (2008) 17361752. doi:10.1016/j.engfracmech.2007.04.010.

[12] Z. Hashin, Finite thermoelastic fracture criterion with application to laminate cracking analysis, Journal of the Mechanics and Physics of Solids. 44 (1996) 11291145. doi:10.1016/0022-5096(95)00080-1.

[13] J.A. Nairn, Exact and variational theorems for fracture mechanics of composites with residual stresses, traction-loaded cracks, and imperfect interfaces, International Journal of Fracture. 105 (2000) 243271.

[14] D. Taylor, P. Cornetti, N. Pugno, The fracture mechanics of finite crack extension, Engineering Fracture Mechanics. 72 (2005) 10211038. doi:10.1016/j.engfracmech.2004.07.001.

[15] P. Weißgraeber, D. Leguillon, W. Becker, A review of Finite Fracture Mechanics: crack initiation at singular and non-singular stress raisers, Archive of Applied Mechanics. (2015). doi:10.1007/s00419-015-1091-7

[16] D. Leguillon, E. Sanchez-Palencia, Computation of singular solutions in elliptic problems and elasticity, Wiley, USA,1987.

[17] D. Leguillon, D. Quesada, C. Putot, E. Martin, Prediction of crack initiation at blunt notches and cavities size effects, Engineering Fracture Mechanics. 74 (2007) 24202436. doi:10.1016/j.engfracmech.2006.11.008.

[18] Z. Yosibash, E. Priel, D. Leguillon, A failure criterion for brittle elastic materials under mixed-mode loading, International Journal of Fracture. 141 (2006) 291312. doi:10.1007/s10704-006-0083-6.

[19] E. Martin, T. Vandellos, D. Leguillon, N. Carrère, Initiation of edge debonding: coupled criterion versus cohesive zone model, International Journal of Fracture. 199 (2016) 157168. doi:10.1007/s10704-016-0101-2.

[20] A. Doitrand, C. Fagiano, F. Hild, V. Chiaruttini, A. Mavel, M. Hirsekorn, Mesoscale analysis of damage growth in woven composites, Composites Part A: Applied Science and Manufacturing. 96 (2017) 7788. doi:10.1016/j.compositesa.2017.02.018.

[21] A. Doitrand, R. Estevez, D. Leguillon, Comparison between cohesive zone and coupled criterion modeling of crack initiation in rhombus hole specimens under quasi-static compression, Theoretical and Applied Fracture Mechanics. 99 (2019) 5159. doi:10.1016/j.tafmec.2018.11.007.

[22] A. Doitrand, R. Estevez, D. Leguillon, Experimental characterization and numerical modeling of crack initiation in rhombus hole PMMA specimens under compression, European Journal of Mechanics - A/Solids. 76 (2019) 290299. doi:10.1016/j.euromechsol.2019.04.013.

[23] E. Martin, D. Leguillon, Energetic conditions for interfacial failure in the vicinity of a matrix crack in brittle matrix composites, International Journal of Solids and Structures. 41 (2004) 69376948. doi:10.1016/j.ijsolstr.2004.05.044.

[24] A. Sapora, P. Cornetti. Crack onset and propagation stability from a circular hole under biaxial loading. International Journal of Fracture. 214 (2018) 97104.

[25] E. Priel, Z. Yosibash, D. Leguillon, Failure initiation at a blunt V-notch tip under mixed mode loading, Int J Fract. 149 (2008) 143173. doi:10.1007/s10704-008-9234-2.

[26] I.G. García, D. Leguillon, Mixed-mode crack initiation at a v-notch in presence of an adhesive joint, International Journal of Solids and Structures. 49 (2012) 21382149. doi:10.1016/j.ijsolstr.2012.04.018.

[27] D. Leguillon, An attempt to extend the 2D coupled criterion for crack nucleation in brittle materials to the 3D case, Theoretical and Applied Fracture Mechanics. 74 (2014) 717. doi:10.1016/j.tafmec.2014.05.004.

[28] A. Doitrand, C. Fagiano, N. Carrère, V. Chiaruttini, M. Hirsekorn, Damage onset modeling in woven composites based on a coupled stress and energy criterion, Engineering Fracture Mechanics. 169 (2017) 189200. doi:10.1016/j.engfracmech.2016.11.021.

[29] A. Doitrand, D. Leguillon, 3D application of the coupled criterion to crack initiation prediction in epoxy/aluminum specimens under four point bending, International Journal of Solids and Structures. 143 (2018) 175182. doi:10.1016/j.ijsolstr.2018.03.005.

[30] E. Martin, D. Leguillon, N. Carrère, A coupled strength and toughness criterion for the prediction of the open hole tensile strength of a composite plate, International Journal of Solids and Structures. 49 (2012) 39153922. doi:10.1016/j.ijsolstr.2012.08.020.

[31] E. Martin, D. Leguillon, O. Sevecek, R. Bermejo, Understanding the tensile strength of ceramics in the presence of small critical flaws, Engineering Fracture Mechanics. 201 (2018) 167175. doi:10.1016/j.engfracmech.2018.06.021.

[32] I.G. García, V. Mantič, A. Blázquez, F. París, Transverse crack onset and growth in cross-ply laminates under tension: application of a coupled stress and energy criterion, International Journal of Solids and Structures. 51 (2014) 38443856. doi:10.1016/j.ijsolstr.2014.06.015.

[33] E. Martin, D. Leguillon, N. Carrère, A twofold strength and toughness criterion for the onset of free-edge shear delamination in angle-ply laminates, International Journal of Solids and Structures. 47 (2010) 12971305. doi:10.1016/j.ijsolstr.2010.01.018.

[34] D. Leguillon, Z. Yosibash, Crack onset at a v-notch. Influence of the notch tip radius, International Journal of Fracture. 122 (2003) 121.

[35] D. Leguillon, E. Sanchez-Palencia, Fracture in heterogeneous materials - Weak and strong singularities. In: Ladevéze P, Zienkiewicz OC, editors. New Advances in computational structural mechanics. Studies in Applied Math 32, Elsevier, Amsterdam, 1992, pp. 423434.

[36] V. Mantič, Interface crack onset at a circular cylindrical inclusion under a remote transverse tension. Application of a coupled stress and energy criterion, International Journal of Solids and Structures. 46 (2009) 12871304. doi:10.1016/j.ijsolstr.2008.10.036.

[37] P. Weißgraeber, S. Hell, W. Becker, Crack nucleation in negative geometries, Engineering Fracture Mechanics. 168 (2016) 93104. doi:10.1016/j.engfracmech.2016.02.045.

[38] A. Carpinteri, P. Cornetti, N. Pugno, A. Sapora, The problem of the critical angle for edge and center V-notched structures, European Journal of Mechanics - A/Solids. 30 (2011) 281285. doi:10.1016/j.euromechsol.2010.12.017.